



Proceeding Paper

Estimating Permafrost Active Layer Thickness (ALT) Biogeography over the Arctic Tundra [†]

Emiliana Valentini ^{1,2,*}, Marco Salvatore ², Serena Sapio ², Roberto Salzano ³, Giovanni Bormidoni ², Andrea Taramelli ^{1,2} and Rosamaria Salvatori ¹

¹ Institute of Polar Sciences of the National Research Council of Italy (ISP CNR), 00015 Rome, Italy; andrea.taramelli@iusspavia.it (A.T.); rosamaria.salvatori@cnr.it (R.S.)

² Institute for Advanced Studies of Pavia (IUSS), 27100 Pavia, Italy; marco.salvadore@uniroma1.it (M.S.); serena.sapio@iusspavia.it (S.S.); giovanni.bormidoni@uniroma1.it (G.B.)

³ Institute of Atmospheric Pollution Research of the National Research Council of Italy (CNR IIA), 50019 Florence, Italy; roberto.salzano@cnr.it

* Correspondence: emiliana.valentini@cnr.it

[†] Presented at the 5th International Electronic Conference on Remote Sensing, 7–21 November 2023; Available online: <https://ecrs2023.sciforum.net/>.

Abstract: The geospatial model here presented estimates the permafrost active layer thickness (ALT) over the entire Arctic in the last 20 years, and it is based on the spatial and temporal oscillations measured by satellite-based essential variables associated with the thermal state of permafrost. The model integrates the climate and soil components, such as the land surface temperature, the snow depth water equivalent, and the mid-summer albedo, with the structural and functional descriptors of Arctic tundra biome such as the fraction of absorbed photosynthetically active radiation. The distribution of estimated ALT varies according to the vegetation classes (mosses and lichens or grasses and shrubs), but a general increase has been estimated across the whole Arctic tundra region, with rates of up to 2 cm/year.

Keywords: permafrost; active layer; model; Arctic amplification; tundra; greening



Citation: Valentini, E.; Salvatore, M.; Sapio, S.; Salzano, R.; Bormidoni, G.; Taramelli, A.; Salvatori, R. Estimating Permafrost Active Layer Thickness (ALT) Biogeography over the Arctic Tundra. *Environ. Sci. Proc.* **2024**, *29*, 13. <https://doi.org/10.3390/ECRS2023-15843>

Academic Editor: Luca Lelli

Published: 11 June 2023



Copyright: © 2023 by the authors. Licensee MDPI, Basel, Switzerland. This article is an open access article distributed under the terms and conditions of the Creative Commons Attribution (CC BY) license (<https://creativecommons.org/licenses/by/4.0/>).

1. Introduction

Permafrost, defined as perennially frozen soil, extends over 15% of the Earth's surface exposed in the northern hemisphere and over the entire Arctic and sub-Arctic region [1]. The layer above of the permafrost is defined as 'active layer' as it freezes in winter and gradually melts in summer, with a resulting thickness that has been estimated to increase as a function of climate change [2,3]. A recent and wide interest has been dedicated to permafrost and to changes that it undergoes due to global warming [4,5]. The importance of studying the effects of permafrost thawing has been underlined in 2021 by the European Union in the 'Joint communication on the Arctic and northern dimension policy' for the Arctic Strategy update. Global warming is triggering heatwaves phenomena at the high latitudes affecting snow freeze/thaw dynamics and leading to earlier snow melting with a consequent lengthening of the snow-off period and of the exposure of land surface to the effects of solar radiation [3,6]. However, the land surface temperature (LST) has been observed to change with a different rate to the air temperature according to the tundra vegetation cover and the associated mid-summer albedo, which is also related to the ALT [7,8]. An increase in temperature during the growing season does not necessarily promote plant growth; rather, it indicates drought stress caused by the lowering of groundwater levels related to the increase in thaw depth [9].

The permafrost freeze/thaw dynamics influence the magnitude of the seasonal vegetation response during the snow-off period, and this phenomenon impacts the permafrost itself [10]. For these reasons, the study of the thermal state of permafrost (TSP) and the

associated ALT involves several essential variables related to vegetation, snow, and soil properties [3].

We present a geospatial model based on Earth Observation (EO) data for estimating biogeographical variation of the permafrost ALT in the Arctic tundra region over the last twenty years. The model integrates essential variables related to the climate and soil components, such as the fraction of the solar radiation absorbed by vegetation via photosynthesis activity (FAPAR) as a descriptor of Arctic tundra vegetation because it depends on canopy structures; the snow depth water equivalent (SDWE) as a proxy of the soil water content because the winter SDWE is strictly related to the summer soil moisture [11]; the albedo as a proxy of the solar radiation reflected back to the atmosphere via land cover, which, in summer, depends on the vegetation cover and the soil saturation [12]; and the LST because it directly impacts the thermal state of permafrost [2,3].

The model develops a holistic approach by weighting the essential variables' trends with the in-situ monitoring of data from the Circumpolar Active Layer Monitoring (CALM) program, which is a component of the Global Terrestrial Network for Permafrost (GTN-P). The result is a set of estimations of ALT over the Arctic tundra biome, and as a directly related product, the frequency distribution of the green component over the entire period provides an estimation of the greening trends and patterns.

2. Methods

The geospatial model is based on the parametrization of each variable for each pixel within the region of interest (Figure 1). As concerns the satellite data, daily MODIS derived products (NASA) of FAPAR (MOD15A2H V6.1), LST (MOD11A1 V6.1), and Albedo (MCD43A3 V6.1) have been involved as variables in the geospatial model, together with the ERA5 hourly reanalysis of SDWE (ECMWF climate).

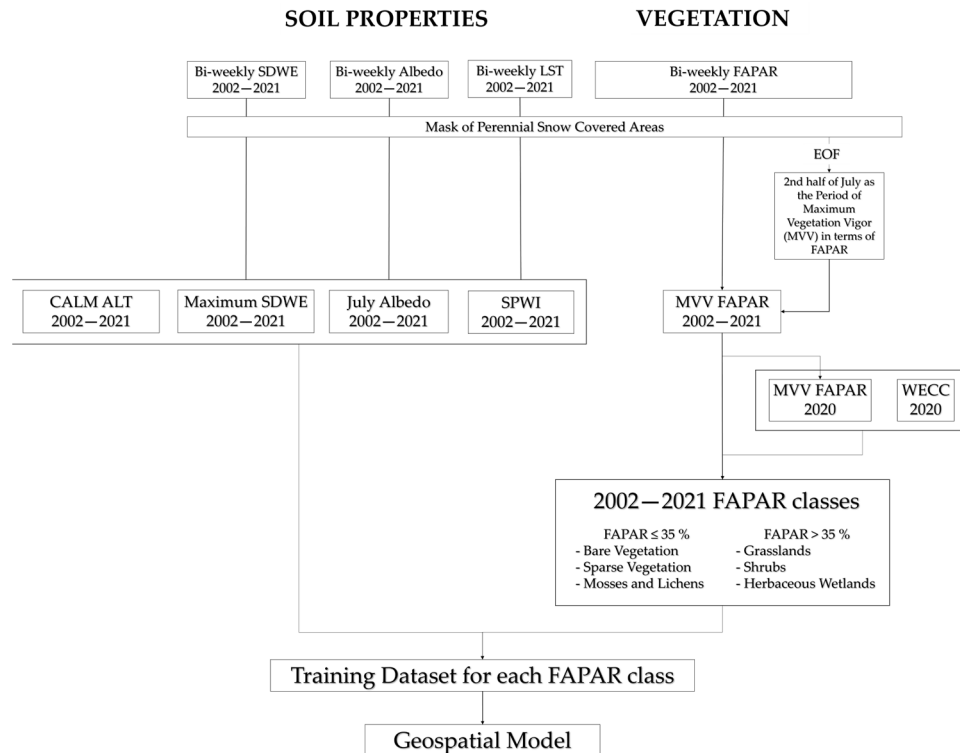


Figure 1. Workflow of the geospatial model for ALT estimations.

Twenty-year (2002–2021) biweekly datasets have been built by considering the average of the MODIS acquisitions in the first and in the last half of each month of the Arctic sunlight period (from March to September) and rescaled at 25 km of spatial resolution. All these datasets have been masked out of the areas covered by ice (from 2020 World ESA

Land Cover Classification) and perennial snow. Perennial snow-covered areas have been identified using MODIS data (MOD10A1.061) with a Normalized Difference Snow Index (NDSI) > 0.4 during the whole time range.

For the Arctic tundra biome classification, the FAPAR dataset has been investigated through empirical orthogonal analysis (EOF)—a statistical technique used to rank spatial and temporal patterns of variability—to identify the maximum seasonal vigor period of the Arctic tundra. Then, the FAPAR dataset has been elaborated to obtain a twenty-year yearly dataset considering the average in the maximum seasonal vigor period previously identified. By overlapping the FAPAR values for the year 2020 with the World ESA Land Cover Classification [13], 2 subzones have been obtained.

For soil properties, the LST dataset has been further elaborated to obtain the yearly Sunlight Period Warmth Index (SPWI), meant as the cumulative sum of the LST monthly means in the sunlight period, while the SDWE and albedo datasets have been elaborated to obtain, respectively, the yearly Maximum value of SDWE (MSDWE) and the July Albedo average (JAlbedo).

Regarding the geospatial model for the estimation of ALT biogeographical variability, this is obtained by building a linear regression model between the yearly SPWI, MSDWE, and JAlbedo and the ALT field data provided by the CALM for each subzone.

These variables generate 2 sets of coefficients on the base of the correlation among them in each FAPAR derived subzone.

The resulting model produced a twenty-year ALT dataset for the Arctic tundra region, and it has been validated through a normal cross-validation, considering the average difference between the estimates and the ground-truth represented by CALM measurements, as well as a spatial cross-validation considering five zones taken by the CALM sites: West Siberia, East Siberia, Alaska, Canada, Greenland and Svalbard. The ALT dataset has been further elaborated to estimate the rate of change in the 2002–2021 period.

3. Results and Discussion

Regarding the Arctic tundra classification, the expansion coefficients (ECs) from EOFs show an oscillation pattern for which the FAPAR maximum values and the related maximum vegetation vigor in the period 2002–2021 have been reached in the second half of July. This temporal pattern also shows that the FAPAR average observed in the Arctic tundra region starts to increase in April—as until March the majority of Arctic surface is covered by snow—and decreases in August. From the analysis of the maximum vegetation vigor (FAPAR maximum values) within the ESA World Cover Classification, two classes have been identified using a threshold of 35% (Figure 2). FAPAR lower than 35% represents areas covered by mosses and lichens and sparse vegetation (subzone A), while areas above this threshold represents herbaceous cover (subzone B) (Figure 3a). The resulting FAPAR classes for the year 2003 have overlapped with the Circumpolar Arctic Vegetation Map (CAVM) [14] of the same year, with an overall accuracy of 71%.

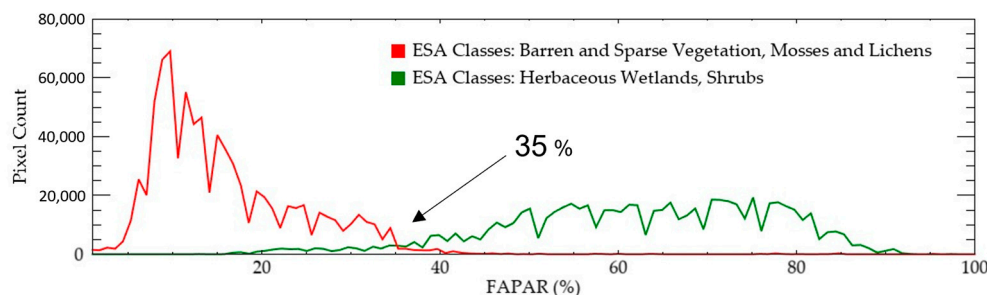


Figure 2. The distribution of FAPAR values in the two classes of land cover obtained by merging the ESA Land Cover 2020 classes.

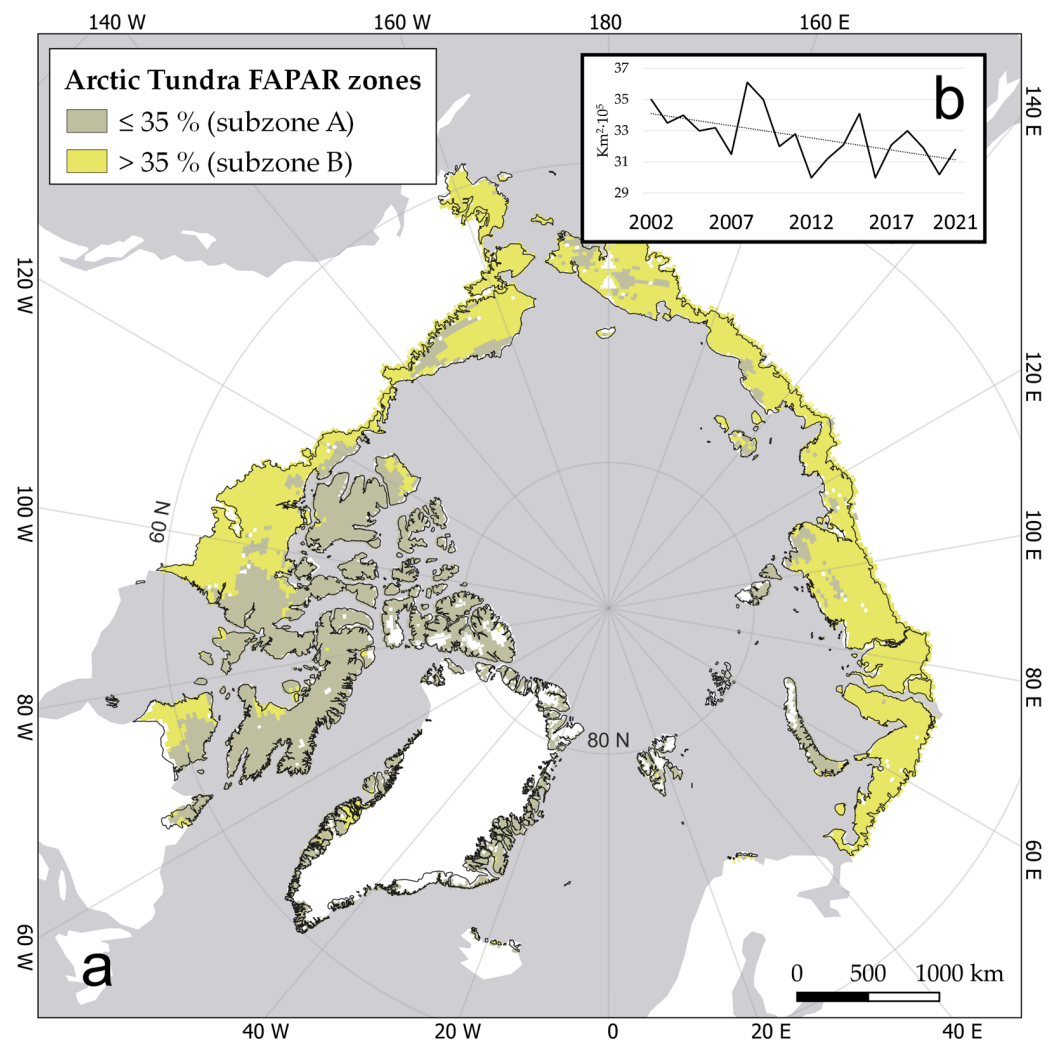


Figure 3. (a) The two Arctic tundra vegetation subzones according to the FAPAR threshold of 35%: mosses and lichens and sparse vegetation ≤ 35% (subzone A); herbaceous cover > 35% (subzone B). (b) The oscillation of the surface of subzone A (km² × 10⁵) over the period 2002–2021, with a dotted line representing the linear intercept of the frequency distribution.

The surface of FAPAR subzone A over the 20 years highlighted a potential progressive reduction (Figure 3b), probably related to the lengthening of the snow off period and to the ephemeral cycle of this kind of vegetation. This trend could also be explained by the associated fractional vegetation cover (FVC). In fact, a lower FVC, typical of the sparse vegetation of high latitudes, could reduce the average FAPAR reported by the mixed pixels.

The model training phase identified the coefficients associated with the independent variables related to the soil properties, respectively, for subzone A (Equation (1)) and subzone B (Equation (2)) for the following resulting equations:

$$ALT = 57.59 \times MSDWE + 22.72 \times JAlbedo + 4.13 \times SPWI + 28.14, \tag{1}$$

$$ALT = 54.85 \times MSDWE + 41.73 \times JAlbedo + 3.06 \times SPWI + 35.03 \tag{2}$$

In Equation (1) are the model coefficients obtained from the parametrization for subzone A, covered by mosses–lichens–sparse vegetation (FAPAR ≤ 35%; R-squared = 0.51); and in the Equation (2), there are the model coefficients obtained for subzone B covered by grasslands–herbaceous wetlands (FAPAR > 35%; R-squared = 0.22). The weight of the MSDWE and SPWI in subzone B is lower than in subzone A. As for MSDWE, this difference

could be because the snowpack is thicker in the areas represented in subzone A and, in turn, the potential water that would come from snow melting and the related impact on ALT is greater than in subzone B. As concerns the SPWI, the difference between the weights in the two equations could be explained by the vegetation type, which is more structured in subzone B; thus, it could better mitigate the temperature impact on the ALT.

Regarding the weight associated with the JAlbedo, the weight in Equation (2) is greater than the weight in Equation (1), probably because of the different vegetation typologies represented in the two subzones: the structured vegetation in subzone B lead to a lower JAlbedo than in subzone A which, in turn, could lead to greater solar radiation absorption with a greater impact on the thermal state of permafrost and the resulting ALT.

The model output is an annual Arctic tundra ALT estimate. As for the accuracy of the result, the cross-validation indicated an error of 9 cm in subzone A and of 8 cm in subzone B. The spatial cross-validation underlined how in subzone A, the resulting estimates have a significant uncertainty in Greenland and Svalbard, while in subzone B, the error is equally distributed over the whole dataset. In the Scandinavian control points, the average error is greater than 15 cm. This error could be due to the lower number of CALM ALT measurements available for the model training. The increases over 20 years show biogeographical patterns spanning from Alaska, with changes up to 60 cm (from 1 m depth in 2002 to 1.6 m in 2021), to Canada, with changes up to 25 cm (from 0.8 m depth in 2002 to 1.05 m in 2021), and Siberia, with changes up to 50 cm (from 0.45 m depth in 2002 to 0.95 m in 2021). The resulting ALT spatial distribution shows a general increase over the whole tundra region, with rates up to around 2 cm/year (Figure 4).

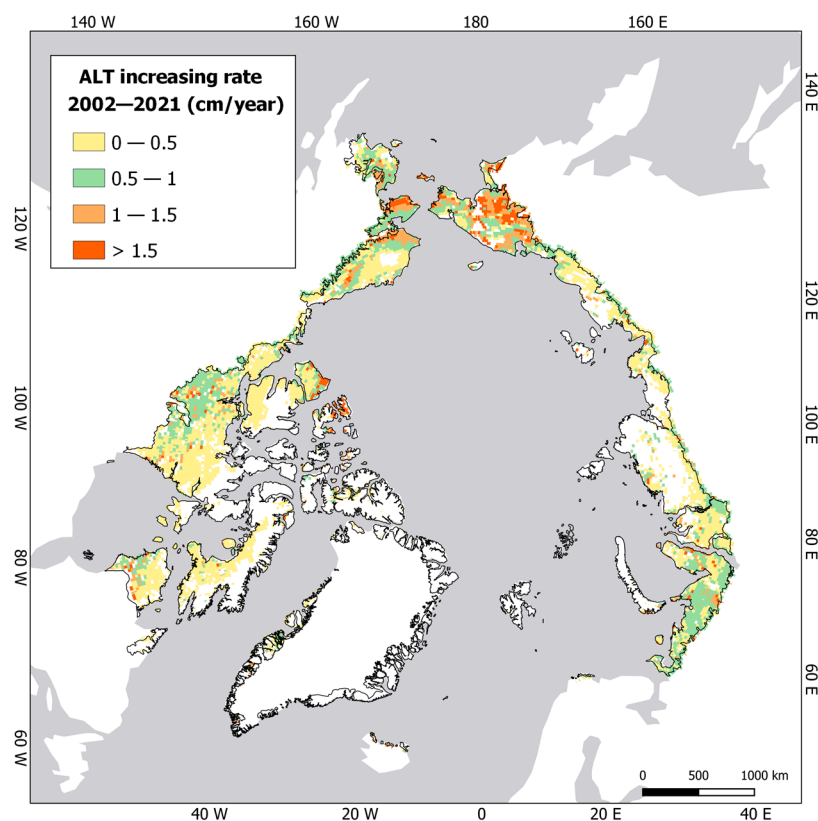


Figure 4. ALT increasing rate calculated as the trend slopes of the linear regression between ALT values and time.

4. Conclusions

The design of the geospatial model here presented demonstrated the opportunity of integrating functional and structural descriptors of vegetation such as FAPAR with other essential variables to estimate the biogeographic variability of the ALT over the

last 20 years. In these terms, the first outcome of the study is the FAPAR classification associated with the vegetation classes, which allows us to confirm the importance of the FAPAR as a descriptor of vegetation typologies but also to open its application in the high Arctic regions. Furthermore, the identification of the two subzones allows us to discuss the differences estimated between the weights of each variable involved in the model and then to investigate the relationships between these variables and the vegetation. The progressive reduction of areas covered by mosses and lichens and sparse vegetation (subzone A) in favor of areas covered by grasses and shrubs (subzone B) could decrease the average albedo, leading to an increase in the solar radiation absorption with climate feedback effects. The model's biogeographical variability highlights some hotspots of ALT, such as Alaska, eastern and western Arctic Siberia, and the southern Arctic Canada.

Author Contributions: Conceptualization, E.V.; methodology, E.V., M.S., S.S. and R.S. (Roberto Salzano); formal analysis, E.V., M.S. and S.S., investigation, E.V., M.S., S.S. and R.S. (Roberto Salzano); resources, A.T., E.V. and R.S. (Roberto Salzano); writing—original draft preparation, M.S., S.S. and E.V.; writing—review and editing, all; supervision, R.S. (Rosamaria Salvatori) and A.T. All authors have read and agreed to the published version of the manuscript.

Funding: This research is partially supported by iSCORE project (PRA_INFRA_2021_9) and by NextGenerationEU, D.M. n. 118/23 del 2 marzo 2023-Accademic Year 2023/2024, Italian National Resilience and Recovery Plan PNRR Missione 4, Componente Investimento 3.4 “Didattica e competenze universitarie avanzate” e Investimento 4.1 “Estensione del numero di dottorati di ricerca e dottorati innovativi per la pubblica amministrazione e il patrimonio culturale” 39° ciclo National Phd Programme in Earth Observation.

Institutional Review Board Statement: Not applicable.

Informed Consent Statement: Not applicable.

Data Availability Statement: The products of this research should be considered under development and they are available for research purposes upon request to the corresponding author.

Conflicts of Interest: The authors declare no conflict of interest.

References

1. Obu, J. How Much of the Earth's Surface is Underlain by Permafrost? *J. Geophys. Res. Earth Surf.* **2021**, *126*, 1–5. [[CrossRef](#)]
2. Meredith, M.; Sommerkorn, M.; Cassotta, S.; Derksen, C.; Ekaykin, A.; Hollowed, A.; Kofinas, G.; Mackintosh, A.; Melbourne-Thomas, J.; Muelbert, M.M.C.; et al. Polar regions. In *IPCC Special Report on the Ocean and Cryosphere in a Changing Climate, SUPPL*; IPCC: Geneva, Switzerland, 2019. [[CrossRef](#)]
3. Trofaier, A.M.; Westermann, S.; Bartsch, A. Progress in space-borne studies of permafrost for climate science: Towards a multi-ECV approach. *Remote Sens. Environ.* **2017**, *203*, 55–70. [[CrossRef](#)]
4. Biskaborn, B.K.; Smith, S.L.; Noetzli, J.; Matthes, H.; Vieira, G.; Streletskiy, D.A.; Schoeneich, P.; Romanovsky, V.E.; Lewkowicz, A.G.; Abramov, A.; et al. Permafrost is warming at a global scale. *Nat. Commun.* **2019**, *10*, 264. [[CrossRef](#)] [[PubMed](#)]
5. Romanovsky, V.E.; Drozdov, D.S.; Oberman, N.G.; Malkova, G.V.; Kholodov, A.L.; Marchenko, S.S.; Moskalenko, N.G.; Sergeev, D.O.; Ukraintseva, N.G.; Abramov, A.A.; et al. Thermal state of permafrost in Russia. *Permafr. Periglac. Process.* **2010**, *21*, 136–155. [[CrossRef](#)]
6. Salzano, R.; Cerrato, R.; Scoto, F.; Spolaor, A.; Valentini, E.; Salvatore, M.; Esposito, G.; Sapio, S.; Taramelli, A.; Salvatori, R. Detection of Winter Heat Wave Impact on Surface Runoff in a Periglacial Environment (Ny-Ålesund, Svalbard). *Remote Sens.* **2023**, *15*, 4435. [[CrossRef](#)]
7. Forzieri, G.; Alkama, R.; Miralles, D.G.; Cescatti, A. Response to Comment on “Satellites reveal contrasting responses of regional climate to the widespread greening of Earth”. *Science* **2018**, *360*, 1180–1184. [[CrossRef](#)] [[PubMed](#)]
8. Plekhanova, E.; Kim, J.-S.; Oehri, J.; Erb, A.; Schaaf, C.; Schaepman-Strub, G. Mid-summer snow-free albedo across the Arctic tundra was mostly stable or increased over the past two decades. *Environ. Res. Lett.* **2022**, *17*, 124026. [[CrossRef](#)]
9. Opała-Owczarek, M.; Piroznikow, E.; Owczarek, P.; Szymański, W.; Luks, B.; Kępski, D.; Szymanowski, M.; Wojtuń, B.; Mięgała, K. The influence of abiotic factors on the growth of two vascular plant species (*Saxifraga oppositifolia* and *Salix polaris*) in the High Arctic. *Catena* **2018**, *163*, 219–232. [[CrossRef](#)]

10. Karlsen, S.R.; Stendardi, L.; Nilsen, L.; Malnes, E.; Eklundh, L.; Julitta, T.; Burkart, A.; Tømmervik, H. Sentinel satellite-based mapping of plant productivity in relation to snow duration and time of green-up (GROWTH). In *SESS Report 2019. The State of Environmental Science in Svalbard—An Annual Report*; SIOS: Longyearbyen, Norway, 2019; Volume 9296, pp. 42–57. Available online: https://www.sios-svalbard.org/sites/sios-svalbard.org/files/common/SESSreport_2019_FullReport-150ppi.pdf (accessed on 20 September 2023).
11. Muñoz-Sabater, J.; Dutra, E.; Agustí-Panareda, A.; Albergel, C.; Arduini, G.; Balsamo, G.; Boussetta, S.; Choulga, M.; Harrigan, S.; Hersbach, H.; et al. ERA5-Land: A state-of-the-art global reanalysis dataset for land applications. *Earth Syst. Sci. Data* **2021**, *13*, 4349–4383. [[CrossRef](#)]
12. Wang, Z.; Kim, Y.; Seo, H.; Um, M.-J.; Mao, J. Permafrost response to vegetation greenness variation in the Arctic tundra through positive feedback in surface air temperature and snow cover. *Environ. Res. Lett.* **2019**, *14*, 044024. [[CrossRef](#)]
13. Zanaga, D.; Van De Kerchove, R.; De Keersmaecker, W.; Souverijns, N.; Brockmann, C.; Quast, R.; Wevers, J.; Grosu, A.; Paccini, A.; Vergnaud, S.; et al. ESA WorldCover 10 m 2020 v100. 2021. Available online: <https://zenodo.org/records/5571936> (accessed on 20 September 2023).
14. Raynolds, M.K.; Walker, D.A.; Balsler, A.; Bay, C.; Campbell, M.; Cherosov, M.M.; Daniëls, F.J.A.; Eidesen, P.B.; Ermokhina, K.A.; Frost, G.V.; et al. A raster version of the Circumpolar Arctic Vegetation Map (CAVM). *Remote Sens. Environ.* **2019**, *232*, 111297. [[CrossRef](#)]

Disclaimer/Publisher’s Note: The statements, opinions and data contained in all publications are solely those of the individual author(s) and contributor(s) and not of MDPI and/or the editor(s). MDPI and/or the editor(s) disclaim responsibility for any injury to people or property resulting from any ideas, methods, instructions or products referred to in the content.